Molecular dynamics study of the binary $Cu_{46}Zr_{54}$ metallic glass motivated by experiments: Glass formation and atomic-level structure

Gang Duan,[1,*] Donghua Xu,[1] Qing Zhang,[2] Guoyun Zhang,[2] Tahir Cagin,[3] William L. Johnson,[1] and William A. Goddard III[2]

[1]*W. M. Keck Laboratory of Engineering Materials, 138-78, California Institute of Technology, 1200 E California Boulevard, Pasadena, California 91125, USA*

[2]*Materials and Process Simulation Center, 139-74, California Institute of Technology, 1200 E California Boulevard, Pasadena, California 91125, USA*

[3]*Department of Chemical Engineering, Texas A&M University, College Station, Texas 77845, USA*

We have identified a binary bulk metallic glass forming alloy $Cu_{46}Zr_{54}$ by analyzing the structure and thermal behaviors of copper mold cast samples using x-ray diffraction, transmission electron microscopy, and differential scanning calorimeter. Motivated by these experimental results, we fitted the effective Rosato-Guillope-Legrand-type force field parameters for the binary Cu-Zr alloy system and the atomistic description of glass formation and structure analysis of the $Cu_{46}Zr_{54}$ alloy based on molecular dynamics simulation will be also presented.

I. INTRODUCTION

Due to their high glass forming ability, good processing ability, and exceptional stability with respect to crystallization along with many promising properties such as high strength, elastic strain limit, fatigue resistance, and corrosion resistance, bulk metallic glasses (BMGs) have acquired considerable attention from scientific as well as technological view points in the last two decades.[1–9] As yet, researchers have developed families of multicomponent systems to be BMG forming alloys: Pd, La, Zr, Mg, Y, Ca, Fe, Ni, and Cu based, and have devoted a large amount of research work trying to obtain basic understandings of these glass forming alloys.[1–4,10–18] Very recently several binary BMGs have been identified in Ca-Al, Cu-Zr, and Cu-Hf alloy systems[12,19–23] by the traditional copper mold casting method, which makes simple binary systems no longer a forbidden area to form bulk amorphous alloys. The discovery of bulk glass formers in binary systems, from an engineering point of view, can provide important guidance to the search for exceptional glass forming alloys and can improve the current alloy developing efficiency significantly.[18] Also simple binary systems might open avenues toward the understanding of fundamental theoretical problems of BMG family alloys.

Molecular dynamics (MD) simulations have been successfully performed to analyze the structural, thermodynamic, and dynamic properties and to investigate the glass forming mechanism of simple Cu-Y, Ni-Zr, Cu-Ag, Cu-Ni, Ni-Mo, Be-Zr, Ni-Zr-Al, Cu-W, Fe-C (B, P), and Cu-Mg amorphous alloys[24–40] at a microscopic level on a scale ranging from the vibration to the mesoscopic times. However, most of these simple binary alloys mentioned above, which showed good glass forming abilities in simulation processes, cannot be fabricated into bulk amorphous samples experimentally. In this paper, to develop a better understanding of the glass formation and to investigate the relationship between properties and liquid structures in metal alloys, we employed MD simulation in conjunction with the quantum Rosato-Guillope-Legrand (RGL)-type many-body force

field[41,42] to examine a Cu-Zr binary alloy. The Cu-Zr model system was particularly chosen because we have discovered that the simple $Cu_{46}Zr_{54}$ alloy could be successfully cast into 2 mm fully amorphous strips by copper mold casting method. X-ray diffraction (XRD), (TEM), and differential scanning calorimetry (DSC) analyses were used to investigate the amorphous structure and the thermal properties of this binary bulk glass former. In addition, for many excellent bulk glass forming alloys, such as Vitreloy 1 ($Zr_{41.2}Ti_{13.8}Cu_{12.5}Ni_{10}Be_{22.5}$) and Vitreloy 4 ($Zr_{47}Ti_8Cu_{7.5}Ni_{10}Be_{27.5}$), if we take the Zr and Ti atoms simply as Zr, and Cu, Ni, and Be atoms simply as Cu, the alloy composition would be $Cu_{45}Zr_{55}$, which is really close to the binary bulk glass former in composition in this work. Therefore, the present alloy $Cu_{46}Zr_{54}$ can play an important role as a model to probe the relationship between the properties and liquid inherent structures for amorphous glassy alloys. Motivated by the experimental progress, we fitted the effective RGL-type force field parameters for the binary Cu-Zr alloy system and used MD simulation to study the glass transition and local structures of this simple metallic glass. It is extremely important to create appropriate interatomic potentials, generate glassy configurations, and study the local structures of the system before we can touch the next step.

We describe the experimental discovery and characterization of the binary bulk glass former in the following section. In Sec. III, we summarize various details of the calculations of the RGL-type many-body force field used to describe the Cu-Zr binary alloy system and the MD approaches used in this paper. Section IV gives the results and discussions obtained from the simulations.

II. BINARY BULK GLASS FORMER $Cu_{46}Zr_{54}$

Ingots of alloys studied in this work were prepared by arc melting mixtures of ultrasonically cleansed 99.999 at. % Cu and 99.9 at. % Zr (crystal bar) pieces on a water cooled copper plate under a Ti-gettered high purity argon atmosphere. Each ingot was flipped over and remelted at least
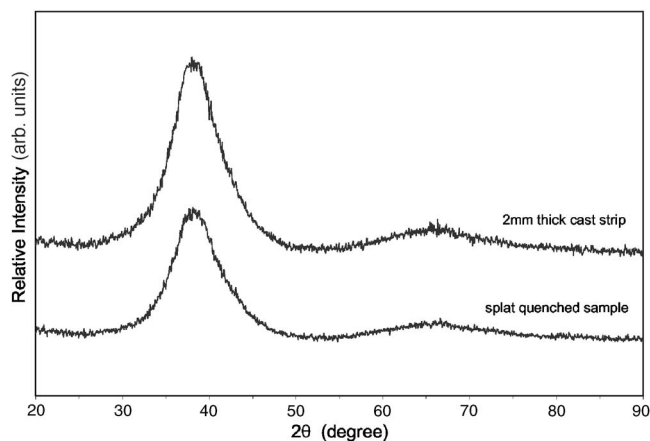
FIG. 1. X-ray diffraction traces of the splat quenched sample and the cross section of the 2 mm thick cast strip of $Cu_{46}Zr_{54}$ alloy.

FIG. 2. DSC scans of the splat quenched sample and the 2 mm thick $Cu_{46}Zr_{54}$ strip at a heating rate of 0.33 K/s.

three times in the arc melter in order to obtain chemical homogeneity. The ingots then were remelted under high vacuum in a quartz tube using an induction heating coil and injected through a ~0.5–1 mm (inner diameter) nozzle into copper molds using high-purity argon at a pressure of ~3–5 atm. Those copper molds used have internal cylindrical cavities of diameters ranging from 0.5 to 3 mm. For comparison purposes, a very thin sample with a thickness ~60 μm was also prepared using an Edmund Buhler D-7400 splat quencher. Both the thin samples and the transverse cross sections of the bulk samples were examined by an x-ray diffractometer (Bruker AXS) using a Cu-Kα source. A Perkin-Elmer DSC7 (differential scanning calorimeter) was utilized for a constant heating rate (dT/dt=0.33 K/s) scanning, aimed at confirming the amorphous structures and studying the glass transition and crystallization behaviors of these alloys, respectively.

Figure 1 shows the x-ray diffraction patterns of the splat quenched sample and the cross section of the 2 mm thick strip. It can be seen clearly that both of them only exhibit a series of broad diffraction maxima with no evidence of any crystalline Bragg peaks, which is a characteristic of amorphous structures. The amorphous state of the as-cast 2 mm thick $Cu_{46}Zr_{54}$ strip was confirmed by the transmission electron diffraction technique, which agrees very well with the x-ray diffraction results presented in Fig. 1.

Thermal analysis was carried out to investigate the glass transition and the crystallization behaviors to understand the amorphous nature of obtained amorphous alloys. Figure 2 presents the DSC scans of the splat quenched sample and the 2 mm thick $Cu_{46}Zr_{54}$ strip at a heating rate of 0.33 K/s, where T_g (glass transition temperature) and T_x (the onset temperature of the first crystallization event) positions are marked with arrows. It shows that each of the traces exhibits a clear endothermic heat event (characteristic of the glass transition) and a distinct undercooled liquid region, followed by exothermic heat release events associated with the crystallization processes.

It is worth noting that the glass forming ability in binary alloy systems has a remarkable sensitivity to the alloy composition. Even a 0.5 at. % change in the composition can
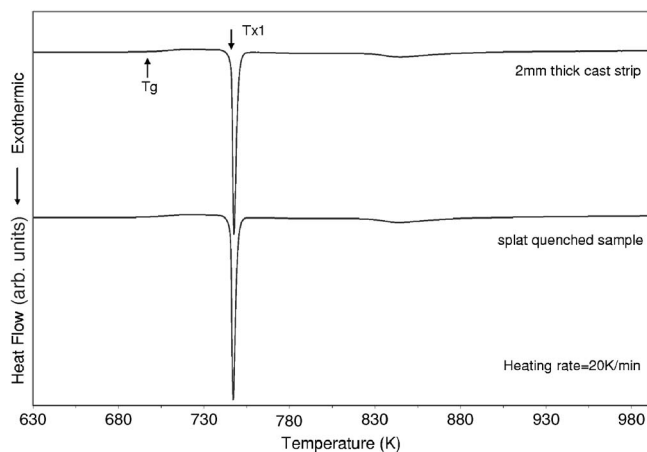
extremely influence the glass forming ability in these binary alloys, which have been shown in Refs. 19 and 20 in the $Cu_{64}Zr_{36}$ vicinity. We also found the similar results in the present work in the vicinity of the $Cu_{46}Zr_{54}$ composition point. Table I lists a summary of properties of the $Cu_{46}Zr_{54}$ bulk amorphous alloy. Several frequently used parameters to evaluate the glass forming ability (GFA) are also calculated: the variations of undercooled liquid region $\Delta T(\Delta T=T_x-T_g)$, the reduced glass transition temperature $T_{rg}(T_{rg}=T_g/T_l$, where T_l is the liquidus temperature) and $\gamma[\gamma=T_x/(T_g+T_l)]$.[43,44]

It is well known that for liquid SiO_2, an extremely low cooling rate (~10^{-3} K/s) is enough to bypass crystallization and retain its amorphous structure after solidification. In contrast, binary metallic liquids have long been considered fragile against crystallization due to their critical high cooling rates of 10^5–10^7 K/s (splat quenching). By using the Fourier heat flow equations, we can estimate the critical cooling rate during the casting process to produce $Cu_{46}Zr_{54}$ binary bulk amorphous samples. If no latent heat due to crystallization is involved, the average cooling rate R at the center of a solidifying liquid is approximately proportional to the inverse square of the smallest mold dimension L, i.e., $R \approx \alpha L^{-2}$ (L in centimeters; R in Kelvin/seconds),[45] where the factor α is related to the thermal diffusivity and the freezing temperature of the liquids (e.g., α~15 Kcm^2/s for Vitreloy 1 $Zr_{41.2}Ti_{13.8}Cu_{12.5}Ni_{10}Be_{22.5}$ alloy). Hence, the cooling rates associated with the formation of the present binary amorphous structures are of the order 10^2–10^3 K/s, significantly lower than what was expected for a typical binary metallic liquid to fully restrain crystallization.

TABLE I. A summary of properties of bulk amorphous $Cu_{46}Zr_{54}$ alloy.

Alloy [in at. %]	Casting diameter [mm]	T_g[K]	T_x[K]	T_l[K][a]	ΔT[K]	T_{rg}	γ
$Cu_{46}Zr_{54}$	2	696	746	1201	50	0.58	0.393

[a]Data taken from Ref. 46.

TABLE II. Rosato-Guillope-Legrand (RGL)-type force field parameters.

	r_0 (Å)	ε(eV)	c(eV)	p	q
Zr-Zr	3.2100	0.3688	2.3365	2.0250	7.9273
Cu-Cu	2.6356	0.2149	1.3483	2.7490	10.2215
Cu-Zr	2.9086	0.3615	2.0100	2.7960	8.6020

According to the Cu-Zr binary phase diagram,[46] $Cu_{46}Zr_{54}$ is associated with one of the eutectic compositions in this binary alloy system. Thermodynamically, the liquid state is more preferable than the ordered solid state in a large region over the eutectic temperature and the energy difference between the two states is relatively small below the eutectic temperature so as to make quenching the liquid to an amorphous state easier. It has been shown that certain atomic size mismatch and efficient atomic packing play an important role in improving the glass forming ability (GFA) of a system.[37,47–49] In the present system, the atomic radii of the components are Zr, 1.58 Å and Cu, 1.27 Å and accordingly $R_{Zr/Cu}=1.244$. Therefore, the present combination of atomic sizes can produce an efficiently packed local structure, which is often associated with low energy and high viscosity of liquids. Another factor that may benefit the GFA has been reported to be large negative heat of mixing among the constituent elements. This criterion is also satisfied since the value of heat of mixing for Zr-Cu is −23 kJ/mol.[50] The large negative heat of mixing enhances the interactions among the components and promotes chemical short range ordering in liquids, which can improve the local packing efficiency and restrain long range diffusion of atoms.

III. MD SIMULATION DETAILS

A. Force field and parameters

The total energy of the system in Rosato-Guillope-Legrand (RGL)-type many-body force field (FF)[41,42] we used in the work has the following form:

$$U_{tot} = \Sigma_i U_i = \Sigma_i [E_B^i + E_R^i],$$

$$E_B^i = -\left\{ \Sigma_{i\neq j} c^2 \mathrm{Exp}\left[-2q\left(\frac{r_{ij}}{r_0} - 1\right)\right]\right\}^{1/2}$$

$$E_R^i = \Sigma_{i\neq j} \frac{1}{2}\varepsilon\, \mathrm{Exp}\left[-p\left(\frac{r_{ij}}{r_0} - 1\right)\right].$$

In these expressions, E_B and E_R denote the many-body metallic bonding potential and the pairwise repulsive energy terms, respectively. r_0 is the first-neighbor distance in the AB lattice and the other four free parameters c, ε, p, q need to be fitted.

We first carried out density functional theory (DFT) quantum mechanics (QM) calculations on various stable and unstable phases (SEQQUEST program[51] was used): pure Cu, Pure Zr, CuZr(B2), Cu_2Zr_2 (layered fcc), CuZr (B1), Cu_3Zr (fcc), and $CuZr_3$ (fcc). The QM results have shown good agreement with the experimental data.[52] The important physical properties were derived from QM and subsequently used as a reference to obtain the force field parameters. We fitted the force field parameters to the QM calculated data such as lattice constants, cohesive energies, and bulk moduli. The obtained force field parameters are shown in Table II for Zr-Zr, Cu-Cu, and Cu-Zr. The comparisons between the FF results and the QM results for each phase of Zr, Cu, and Cu-Zr are made in Table III–V, respectively. As we expect, the RGL-type force field describes Cu-Zr alloys quite well and is suitable for studying Cu-Zr binary metallic glasses using MD simulation. From the RGL-type potential expressions, we notice that the atomic interactions decay exponentially with the increase of atomic spacing. Hence, it is applicable to set the cut-off distance as short as to include only two shells of atoms. In this work, we take the cut-off distance as 4.5 Å.

B. Molecular dynamics

The simulations in this work are based on a constant temperature, constant thermodynamic tension (TtN) MD method.[53] This method combines the Nose canonical ensemble[54] with the Parrinello-Rahman variable shape size ensemble[55,56] and can capture very detailed microscopic information about the system, allowing us to study the phase transformation while permitting the shape and size of the cell to change. We can obtain the data of volume, structure, and energy comparable with experimental data with an accurate force field.

We started our MD simulations from a super cell box with 2000 atoms (Composition $Cu_{46}Zr_{54}$) under periodic boundary conditions. To generate the exact composition, we randomly substituted 80 copper atoms with the same amount of zirco-

TABLE III. A comparison between RGL-type force field and QM results for Zr.

Phase	E_ff[eV/atom]	E_qm[eV/atom]	ΔE[%]	Ω_ff[Å³]	Ω_qm[Å³]	$\Delta\Omega$[%]
fcc	−6.21	−6.21	0.00	23.56	23.56	0.00
hcp	−6.21	−6.25	0.64	23.56	23.22	1.46
bcc	−6.04	−6.17	2.11	23.95	23.30	2.79
$A15$	−6.02	−6.10	1.31	24.18	23.33	3.64
SC	−5.75	−5.29	8.70	26.14	24.65	6.04
DM	−4.85	−3.56	36.24	34.84	32.01	8.84

TABLE IV. A comparison between RGL-type force field and QM results for Cu.

Phase	E_*ff*[eV/atom]	E_*qm*[eV/atom]	ΔE[%]	Ω_*ff*[Å^3]	Ω_*qm*[Å^3]	$\Delta\Omega$[%]
fcc	−3.49	−3.49	0.00	12.90	12.94	0.31
hcp	−3.49	−3.44	1.45	12.69	12.76	0.55
bcc	−3.42	−3.48	1.72	13.07	13.01	0.46
*A*15	−3.36	−3.38	0.59	13.35	13.32	0.23
SC	−3.09	−3.03	1.98	15.20	14.50	4.83
DM	−2.58	−2.45	5.31	21.58	20.84	3.55

nium atoms in the B2 structure (Cu$_{50}$Zr$_{50}$ with 2000 atoms). The TtN MD simulations were carried out in a series of increasing temperatures from 0 to 2400 K (a temperature several hundred degrees higher than the melting point) in 100 K increments. At each temperature the MD simulation time step was taken as 1 fs (10^{-15} s) and the simulation time for determining the properties was 20 ps (10^{-12} s). After equilibrating the structure in the liquid phase, we cooled the system using three different quenching rates from 2.5, 5, and 10 K/ps from 2400 K down to 100 K in 100 K decrements in the TtN ensemble. To achieve the set cooling rate, we kept the model system at the same temperature for times of 40, 20, and 10 ps.

IV. MD SIMULATION RESULTS AND DISCUSSIONS

A. Glass transition

Figure 3 presents the variation of volume as a function of temperature during the heating and cooling cycles. There is a noticeable jump in volume beginning from about 1400 K for the heating process, signifying the melting of the model. We can also observe the overlap stage between the heating and cooling curves, which indicates that our simulation system was melted. The reasons that we have a higher melting temperature than the equilibrium value might be the homogeneous model system without a free surface and the high heating rate.

From the cooling curve, we observe that there is a continuous change in volume compared with the heating process and no dramatic drop in the volume upon the whole cooling. However, the slope of the volume versus temperature curve decreases below 700 K, which is a sign of glass formation. As is well known, the glass transition is not a true thermodynamic second order phase transition since T_g is not fixed but depends on experimental conditions, particularly the

cooling rate. At around the glass transition temperature, changes in volume, enthalpy, and entropy are continuous and have a change in slope at T_g, but their derivatives such as heat capacity and thermal expansion coefficient are discontinuous. We also investigated the effect of different cooling rates on the glass transition temperature. Figure 4 shows the volume versus temperature curves at three different quenching rates, 2.5, 5, and 10 K/ps, which reveals the cooling rate dependence of glass transition temperature. The faster cooling rate results in shorter times for the atoms to relax, thus leading to a higher glass transition temperature. In the present work we can observe the similar trend; however there is only a slight difference among the glass transition temperatures.

A parameter often used to be the measure of the phase transition (to glass or crystal) is the Wendt-Abraham (WA) parameter[57] extracted from the radial distribution function, which is defined by $R^{WA} = g_{min}/g_{max}$. Here g_{min} and g_{max} are the values of the radial distribution function $g(r)$ at the first minimum and the first maximum. The Wendt-Abraham parameter stresses the local character of $g(r)$, permitting a direct comparison between structures and leading to a sensitive estimation of glass transition temperatures. We notice from our calculation that the temperature dependence of the Wendt-Abraham parameter R^{WA} leads to a clear intersection between two straight lines at $T_g = 700$ K, which is consistent with the one obtained from the volume versus temperature curve.

B. Radial distribution function

Radial distribution function (RDF) analysis is among one of the most important methods to reveal the structure features of a system, particularly for liquids and amorphous structures. The RDF can be calculated as

TABLE V. A comparison between RGL-type force field and QM results for Cu-Zr system.

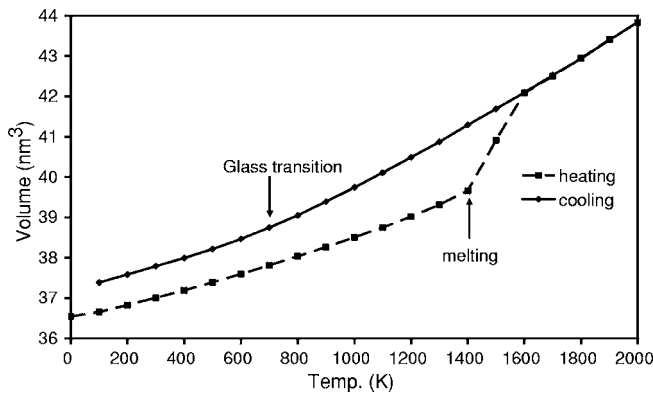| Phase	E_*ff*[eV/atom]	E_*qm*[eV/atom]	ΔE[%]	Ω_*ff*[Å^3]	Ω_*qm*[Å^3]	$\Delta\Omega$[%]
CuZr (*B*2)	−5.03	−5.03	0.00	17.64	17.85	1.18
Cu$_2$Zr$_2$ (Layered fcc)	−5.09	−4.96	2.62	17.48	17.71	1.30
CuZr (*B*1)	−4.94	−4.65	6.24	19.79	19.69	0.51
Cu$_3$Zr (fcc)	−4.75	−4.11	15.57	14.60	15.83	7.77
CuZr$_3$ (fcc)	−5.57	−5.56	0.18	20.58	20.31	1.33

FIG. 3. Volume as a function of temperature of $Cu_{46}Zr_{54}$ during the heating and cooling at a rate of 5 K/ps.

$$g(r) = \frac{V}{N^2} \left\langle \sum_{i=1}^{n} \frac{n(r)}{4\pi r^2 \Delta r} \right\rangle,$$

where N denotes the number of atoms in the simulation cell, V is the volume of the same cell, and $n(r)$ the number of particles which can be found in the shell from r to $r+\Delta r$. For the binary alloy system in this work, partial radial distribution function (PRDF) for atom α and atom β is calculated by

$$g_{\alpha\beta}(r) = \frac{V}{N_\alpha N_\beta} \left\langle \sum_{i=1}^{N_\alpha} \frac{n_{i\beta}(r)}{4\pi r^2 \Delta r} \right\rangle.$$

Figure 5 presents the PRDF of the model structure at different temperatures (400 K heating, 2000 K liquid state, and 400 K cooling) during the heating and cooling processes. We started our simulation from the random $B2$ structure, which can be seen clearly from the PRDF at 400 K in Fig. 5(a). It shows the typical peaks of a $B2$ structure at $\sigma, 1.16\sigma, 1.67\sigma, 1.96\sigma, 2\sigma$, where σ is the first-nearest-neighbor distance. Also we can observe from the PRDF that the first-nearest-neighbor positions are occupied by unlike atoms only and the second-nearest-neighbor positions are occupied by like atoms only. However, at 2000 K the emer-
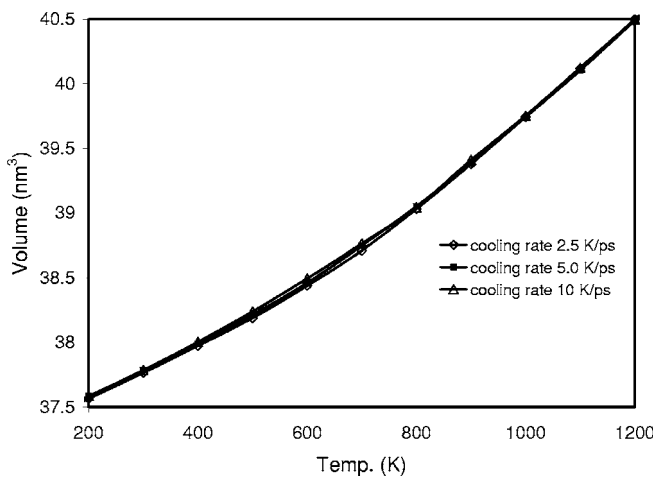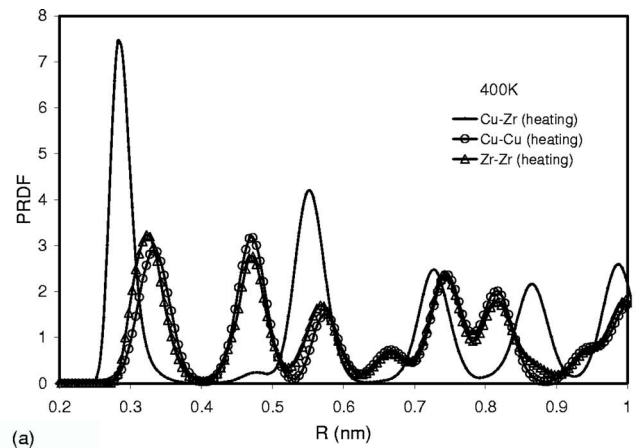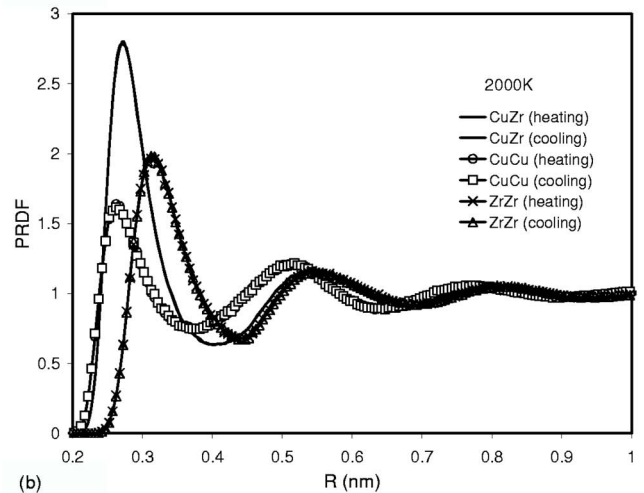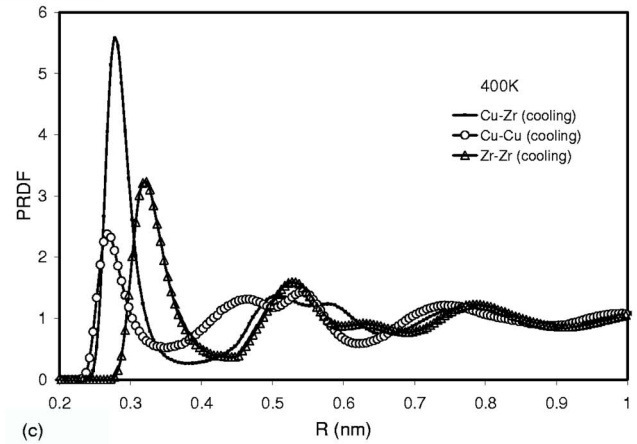

FIG. 4. Volume versus temperature curves for $Cu_{46}Zr_{54}$ obtained from three different quenching rates.

FIG. 5. Partial radial distribution function (PRDF) of $Cu_{46}Zr_{54}$ for different bond pairs during the heating and cooling processes at the rate of 5 K/ps, (a) 400 K heating process, (b) 2000 K in liquid state, and (c) 400 K cooling process.

gence of broad peaks in the PRDF [Fig. 5(b)] shows that the structure has melted and is in a liquid state. For instance, $g(r)_{Cu-Cu}$ indicates a peak at the first-nearest-neighbor distance 2.6 Å, which is close to the value in the liquid state of the pure element. Upon cooling to 400 K at the rate of 5 K/ps, we can also see that the feature of long range disorder in the PRDF [Fig. 5(c)] and the second peaks of $g(r)_{Cu-Zr}$,
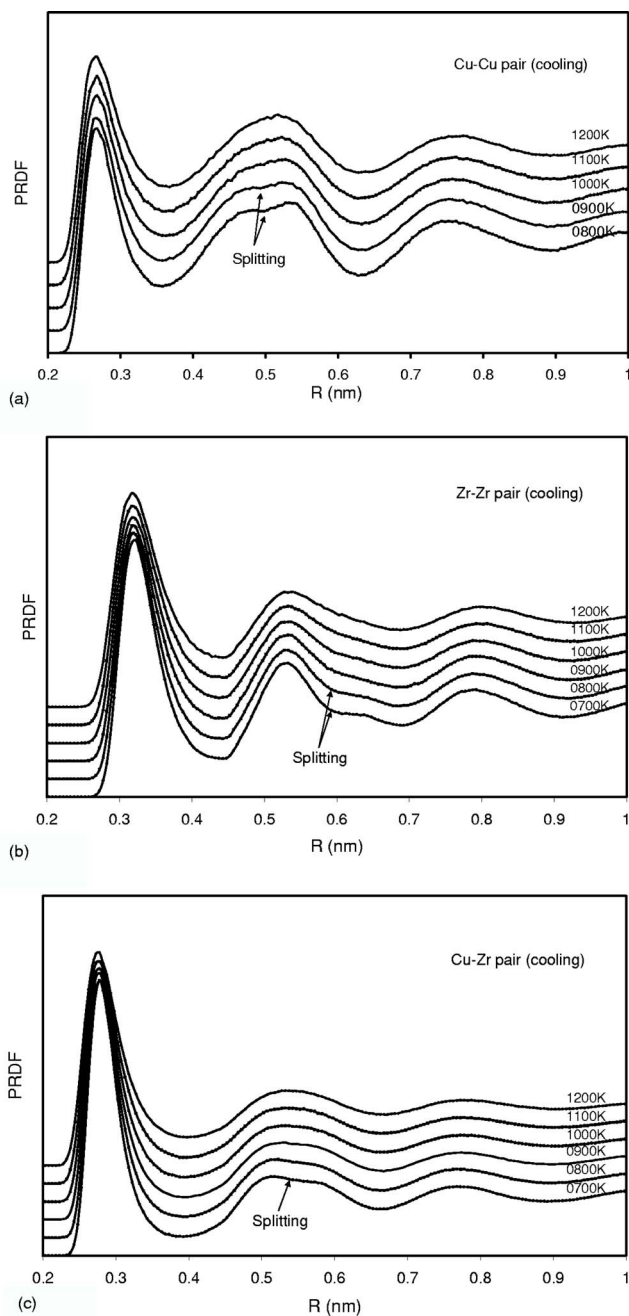
FIG. 6. PRDF of $Cu_{46}Zr_{54}$ for different bond pairs during the cooling cycle at the rate of 5 K/ps, (a) Cu-Cu pair, (b) Zr-Zr pair, and (c) Cu-Zr pair.

TABLE VI. First peak positions from different techniques for amorphous Cu-Zr alloys.

	$R(Cu\text{-}Cu)$[Å]	$R(Cu\text{-}Zr)$[Å]	$R(Zr\text{-}Zr)$[Å]
$Cu_{50}Zr_{50}$ (XRD)[a]	2.53	2.75	3.15
$Cu_{46}Zr_{54}$ (EXAFS)[b]	2.54	2.72	3.14
$Cu_{46}Zr_{54}$[c]	2.67	2.78	3.22

[a]Reference 59.
[b]Reference 60.
[c]This work.

rates used in this work and similar PRDF distributions have been obtained.

As we have mentioned above, we can distinguish splittings of the second peaks in all three PRDFs. However, the splitting occurs at different temperatures for $g(r)_{Cu\text{-}Cu}$, $g(r)_{Cu\text{-}Zr}$, and $g(r)_{Zr\text{-}Zr}$. Figure 6 displays the PRDFs of Cu-Cu, Cu-Zr, and Zr-Zr pairs at different temperatures during the cooling cycle. We notice that for the Cu-Cu pair, the splitting is already well developed at T_g and in fact it first occurs at about 900 K [Fig. 6(a)], which is well above T_g (the temperature T_{split} is determined somewhat by visual inspection of the PRDF's at different temperatures). While for Zr-Zr and Cu-Zr pairs, the splittings occur at lower temperatures, which are 800 and 700 K, respectively. This reveals that some substructures have formed in like atom pairs before reaching the final glassy state.

The local structure of metallic glasses in the binary Cu-Zr system has been studied experimentally using x-ray diffraction and extended x-ray-absorption fine structure (EXAFS) techniques.[59,60] In these papers, the glassy samples were prepared by melt quenching or levitation melting, which should achieve a cooling rate of the order of 10^6 K/s. Table VI lists the first peak positions of PRDFs obtained from three different techniques, x-ray diffraction, EXAFS, and calculation at room temperature. Note that the data represents two remarkably different cooling rates, the order of 10^6 K/s for XRD and EXAFS data and the order of 10^{12} K/s for the present simulation work. Our model system in simulation has larger nearest-neighbor distances than those from experiments. According to the Cohen-Grest free volume theory,[61] upon cooling a glass forming material from the liquid state, some excess quenched-in free volume will be trapped into the glassy state, the quantity of which depends on the cooling rate. The higher cooling rate, the larger free volume in the final glassy state and thus the larger nearest-neighbour distances in the atom pairs.

$g(r)_{Cu\text{-}Cu}$, and $g(r)_{Zr\text{-}Zr}$ are distinctly split as well, showing the formation of an amorphous phase.[58] The first peak of unlike pairs is relatively sharp compared with those of like atom pairs, which qualitatively suggests a preferred interaction of unlike atom pairs in this alloy. According to our calculations, the second peak splittings show up at $1.8\sigma_1$ and $2.08\sigma_1$ for the Cu-Zr pair, at $1.75\sigma_2$ and $2.03\sigma_2$ for the Cu-Cu pair, and $1.64\sigma_3$ and $1.95\sigma_3$ for the Zr-Zr pair, respectively, where σ_1, σ_2, and σ_3 are the first peak positions. Thus quenching the $Cu_{46}Zr_{54}$ alloy from the liquid to 100 K at the rate of 5 K/ps leads to the formation of a metallic glass. We also examined the PRDF for the other two different cooling

C. Coordination Numbers

As is known, the coordination number is defined as the number of atoms bounded to a given atom in a structure. By integrating the partial radial distribution function appropriately, we can determine the partial, total, and average coordination numbers Z_{AB}, Z_A, and Z (the cut-off distance for the integration is taken as the first minimum point in PRDF). These are shown in Fig. 7, for different temperature PRDFs from the cooling run. The average coordination number is
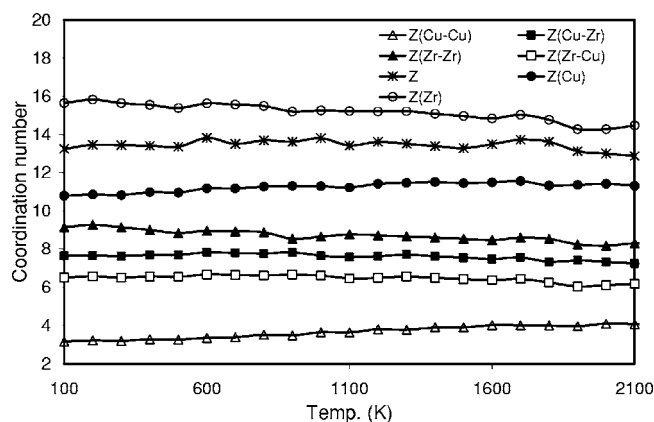
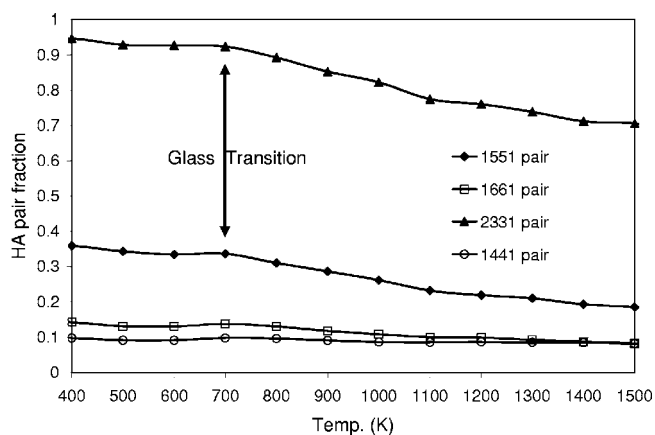FIG. 7. Partial, total, and average coordination numbers of $Cu_{46}Zr_{54}$ calculated for the cooling cycle with the rate of 5 K/ps.

FIG. 8. Variation of the fractions of Honeycutt-Andersen indices during the cooling cycle at the rate of 5 K/ps.

quite independent of temperature change, $Z = 13.27 \pm 0.54$. The coordination number of Zr is always higher than the average Z, and Z_{Cu} always lower.

The numbers of nearest-neighbor correlations extracted from three different techniques are listed in Table VII. We observe that the values indicate more or less random distribution of metal atoms in amorphous Cu-Zr alloys, although a negative heat of mixing suggests the preferred atomic bonding of unlike atom pairs.

D. Honeycut-Anderson analysis

The absence of long-range order is the well-known characteristic of the atomic arrangement in amorphous structures. However, it is difficult to determine details of the atomic arrangement with the structure-probing techniques such as x-ray diffraction due to the absence of long parallel rows and flat parallel planes of atoms in glasses. For such systems, Honeycutt and Andersen (HA) analysis has been proved to successfully assess local structures of amorphous phases.[62–69,37] In this method, pairs of atoms are classified by: (i) whether or not they are near neighbors; (ii) the number of near neighbors they have in common; and (iii) the near-neighbor relationships among the shared neighbors. Therefore, a sequence of four integers ($ijkl$) is designed to characterize the local structure. The first integer i is to identify the bonding of two given atoms. i is 1 when they are bonded in the root pair, otherwise i is 2; the second integer j is the number of the near neighbors shared in common by the

TABLE VII. The numbers of near neighbor correlations obtained from different techniques.

	N (Cu-Cu)	N (Cu-Zr)	N (Zr-Cu)	N (Zr-Zr)
$Cu_{50}Zr_{50}$ (XRD)[a]	5.8	5.6	5.0	5.0
$Cu_{46}Zr_{54}$ (EXAFS)[b]	6.0	5.5	5.0	5.0
$Cu_{46}Zr_{54}$[c]	3.2	7.6	6.5	9.1

[a]Reference 59.
[b]Reference 60.
[c]This work.

two given atoms; the third integer k is the number of bonds among the shared neighbors; the fourth integer l is needed to differentiate between the cases when the first three indices are same but the bond geometries are different. To determine whether or not two atoms are bonded, we use the first minimum in the PRDF for the particular pair of atoms at the temperature being calculated as the cutoff distance. Also the pair fractions of HA indices are normalized just for convenience so that the sum over all cases for nearest neighbors ($i=1$) adds up to unity.

Different structures have different HA indices and general observations are as follows: the face-centered cubic (fcc) structure leads only to 1421; the hexagonal close packed (hcp) structure leads to 50% 1421 and 50% 1422; the 13-atom icosahedron structure has 71% 1321, 29% 1551, and also 71% 2331 while the binary bcc ($B2$) structure has 43% 1441 and 57% 1661, if A-A and B-B bonds are considered in addition to A-B bonds. In general, 1421 and 1422 are characteristics of the closest packed crystalline structures (fcc and hcp). 1441 and 1661 are characteristics of the $B2$ structure while 1551 and 2331 are characteristics of icosahedral ordering.

We first calculated the HA pair fractions for the beginning structure. The results show that this simulation cell leads to 42% 1441, 56% 1661 and the fractions of 1551 pairs and 2331 pairs are almost zero, which confirms our beginning random $B2$ structure. Upon heating to 1200 K before melting, the 1441 and 1661 pair fractions gradually decrease to 29% and 37%, respectively, although these two pairs are still the main components of the local structures. After melting at 2000 K, 1441 and 1661 drop to 7% and 6%, respectively, while 1431, 1541, and 1551 increase to 16%, 12%, and 14%, respectively, showing the structure of a liquid state.

Figure 8 shows the HA pair fractions as a function of temperature when the binary $Cu_{46}Zr_{54}$ system was cooled down from 1500 to 400 K. We can observe that in the cooling simulation the 1441 and 1661 pairs do not change much in the whole temperature range. The 1441 pair fraction changes from about 8% at 1500 K to 10% at 700 K (glass transition temperature) and then remains almost constant till 400 K. The 1661 pairs follow the behavior of 1441, reaching to 8% at 1500 K supercooled liquid state, increasing to 14%

at T_g, and being nearly unchanged until 400 K. In contrast, the icosahedral 1551 and 2331 pairs increase uniformly as the system supercools until local maxima at 700 K of 92% of 2331 and 34% for 1551 are reached, indicating the final state after quenching with a cooling rate of 5 K/ps is amorphous. Therefore, as the model system is cooled from its liquid state, the icosahedral symmetry keeps increasing until the model system reaches the phase transition point. Recently the short range order structures of amorphous solids have been characterized in kinds of metallic glasses by neutron diffraction and EXAFS, etc., local environmental probing techniques.[70–74] The evidence of icosahedral short range order in $Zr_{70}Cu_{30}$ and $Zr_{70}Cu_{29}Pd_1$ has been reported[71] and it supports the theory claiming a correlation between the existence of local icosahedral short range order and the stability of the supercooled liquid state. It has also been shown that the icosahedral topological local order develops to a very high degree even in amorphous Ni-Ag alloy with no tendency to form quasicrystals.[73] The HA index analysis of $Cu_{46}Zr_{54}$ metallic glass in the present work is in good agreement with these experimental progress.

CONCLUDING REMARKS

For a simple binary $Cu_{46}Zr_{54}$ alloy, fully amorphous strip-shaped samples with thickness up to 2 mm were successfully synthesized by the traditional copper mold casting method. The cooling rate associated with the $Cu_{46}Zr_{54}$ bulk glass formation was estimated to be as low as the order of 10^2–10^3 K/s. Several factors based on empirical rules related to bulk metallic glass formation such as eutectic composition, atomic size mismatch, and large negative heat of mixing have been discussed.

An effective tight bonding RGL-type n-body force field for the binary Cu-Zr alloy system was constructed and employed in MD simulations. Partial radial distribution functions, coordination numbers, and Honeycutt-Andersen (HA) indices have been calculated to analyze the local structures of $Cu_{46}Zr_{54}$ metallic glass. Distinct splittings of the second peaks have been observed in all three Cu-Cu, Cu-Zr, and Zr-Zr PRDFs and the splittings occur at different temperatures for different atom pairs. The higher cooling rate from the MD simulation results in larger free volume and accordingly larger nearest-neighbor distances in the atom pairs compared with those from experiments. HA index analysis reveals a high degree of the local icosahedral fivefold short range order structure in the present MD glassy alloy. The MD simulation can bring us much useful information about the local structure of amorphous alloys; one should also notice the large difference in the cooling rate between the MD glass and that obtained from the casting experiments.

---

*Author to whom correspondence should be addressed; email address: duan@its.caltech.edu.

[1] A. L. Drehman, A. L. Greer, and D. Turnbull, Appl. Phys. Lett. **41**, 716 (1982).

[2] A. Inoue, T. Zhang, and T. Masumoto, Mater. Trans., JIM **31**, 425 (1990).

[3] T. Zhang, A. Inoue, and T. Masumoto, Mater. Trans., JIM **32**, 1005 (1991).

[4] A. Peker and W. L. Johnson, Appl. Phys. Lett. **63**, 2342 (1993).

[5] W. L. Johnson, Mater. Res. Bull. **24**, 42 (1999).

[6] A. Inoue and A. Takeuchi, Mater. Trans., JIM **43**, 1892 (2002).

[7] J. Basu and S. Ranganathan, Sadhana - Acad. Proc. Eng. Sci. **28**, 783 (2003).

[8] J. F. Löffler, Intermetallics **11**, 529 (2003).

[9] W. H. Wang, C. Dong, and C. H. Shek, Mater. Sci. Eng., R. **44**, 45 (2004).

[10] A. Inoue, A. Kato, T. Zhang, S. G. Kim, and T. Masumoto, Mater. Trans., JIM **32**, 609 (1991).

[11] F. Q. Guo, S. J. Poon, and G. J. Shiflet, Appl. Phys. Lett. **83**, 2575 (2003).

[12] F. Q. Guo, S. J. Poon, and G. J. Shiflet, Appl. Phys. Lett. **84**, 37 (2004).

[13] Z. P. Lu, C. T. Liu, J. R. Thompson, and W. D. Porter, Phys. Rev. Lett. **92**, 245503 (2004).

[14] V. Ponnambalam, S. J. Poon, and G. J. Shiflet, J. Mater. Res. **19**, 1320 (2004).

[15] V. Ponnambalam, S. J. Poon, and G. J. Shiflet, J. Mater. Res. **19**, 3046 (2004).

[16] H. Choi-Yim, D. H. Xu, and W. L. Johnson, Appl. Phys. Lett. **82**, 1030 (2003).

[17] D. Xu, G. Duan, and W. L. Johnson, Acta Mater. **52**, 3493 (2004).

[18] D. H. Xu, G. Duan, and W. L. Johnson, Phys. Rev. Lett. **92**, 245504 (2004).

[19] D. Wang, Y. Li, B. B. Sun, M. L. Sui, K. Lu, and E. Ma, Appl. Phys. Lett. **84**, 4029 (2004).

[20] D. H. Xu, B. Lohwongwatana, G. Duan, W. L. Johnson, and C. Garland, Acta Mater. **52** 2621 (2004).

[21] M. B. Tang, D. Q. Zhao, M. X. Pan, and W. H. Wang, Chin. Phys. Lett. **21**, 901 (2004).

[22] G. Duan, D. H. Xu, and W. L. Johnson, Metall. Mater. Trans. A **36A**, 455 (2005).

[23] A. Inoue, W. Zhang, and J. Saida, Mater. Trans., JIM **45**, 1153 (2004)

[24] R. Frattini and R. G. DellaValle, Phys. Rev. B **50**, 3620 (1994).

[25] H. Teichler, Phys. Rev. Lett. **76**, 62 (1995).

[26] T. Aihara, Y. Kawazoe, and T. Masumoto, J. Non-Cryst. Solids **207**, 875 (1996).

[27] R. R. Nurgayanov and V. G. Chudinov, Glass Phys. Chem. **23**, 400 (1997).

[28] Y. Qi, T. Cagin, Y. Kimura, and William A Goddard, III, Phys. Rev. B **59**, 3527 (1999).

[29] Z. C. Li and B. X. Liu, Chin. Phys. Lett. **16**, 667 (1999).

[30] M. I. Mendelev, S. N. Ishmaev, F. Hajdu, G. Meszaros, and E. Svab, Mater. Sci. Forum **321**, 496 (2000).

[31] H. Teichler, J. Non-Cryst. Solids **293**, 339 (2001).

[32] M. Guerdane and H. Teichler, Phys. Rev. B **65**, 014203 (2002).

[33] K. Brinkmann and H. Teichler, Phys. Rev. B **66**, 184205 (2002).

[34] Y. Qi, T. Cagin, Y. Kimura, and W. A. Goddard, J. Comput.-Aided Mater. Des. **8**, 233 (2002).

[35] H. R. Gong, L. T. Kong, W. S. Lai, and B. X. Liu, Phys. Rev. B **68**, 144201 (2003).

[36] A. V. Evteev, A. T. Kosilov, and E. V. Levtchenko, Acta Mater. **51**, 2665 (2003).

[37] H.-J. Lee, T. Cagin, W. L. Johnson, and W. A. Goddard, J. Chem. Phys. **119**, 9858 (2003).

[38] N. P. Bailey, J. Schiotz, and K. W. Jacobsen, Phys. Rev. B **69**, 144205 (2004).

[39] M. Shimono and H. Onodera, Mater. Trans., JIM **45**, 1163 (2004).

[40] F. Albano, N. Lacevic, M. L. Falk, and S. C. Glotzer, Mater. Sci. Eng., A **375–77**, 671 (2004) special issue.

[41] V. Rosato, M. Guillope, and B. Legrand, Philos. Mag. A **59**, 321 (1989).

[42] F. Cleri and V. Rosato, Phys. Rev. B **48**, 22 (1993).

[43] Z. P. Lu and C. T. Liu, Phys. Rev. Lett. **91**, 115505 (2003).

[44] Z. P. Lu, C. T. Liu, Acta Mater. **50**, 3501 (2002).

[45] W. L. Johnson (unpublished).

[46] *Binary Alloy Phase Diagrams*, 2nd ed., edited by T. B. Massalski ASM (Metals Park, OH, Int. 1990).

[47] T. Egami and Y. Waseda, J. Non-Cryst. Solids **64**, 113 (1984).

[48] D. B. Miracle, W. S. Sanders, and O. N. Senkov, Philos. Mag. A **83**, 2409 (2003).

[49] D. B. Miracle, Nat. Mater. **3**, 697 (2004).

[50] F. R. de Boer, R. Boom, W. C. M. Matterns, A. R. Miedema, and A. K. Niessen, *Cohesion in Metals* (North-Holland, Amsterdam, 1988).

[51] P. A. Schultz, Sandia National Laboratories; for more information, please check http://www.cs.sandia.gov/˜paschul/Quest/

[52] H. -J. Lee, Ph.D. thesis, California Institute of Technology, 2003.

[53] J. R. Ray and A. Rahman, J. Chem. Phys. **82**, 4243 (1985).

[54] S. Nose, Mol. Phys. **52**, 255 (1984); S. Nose, J. Chem. Phys. **81**, 511 (1984).

[55] M. Parrinello and A. Rahman, Phys. Rev. Lett. **45**, 1196 (1980).

[56] M. Parrinello and A. Rahman, J. Appl. Phys. **52**, 7182 (1981).

[57] H. R. Wendt and F. F. Abraham, Phys. Rev. Lett. **41**, 1244 (1978).

[58] J. L. Finney, Nature (London) **266**, 309 (1977).

[59] H. S. Chen and Y. Waseda, Phys. Status Solidi A **51**, 593 (1979).

[60] A. Sadoc, Y. Calvayrac, A. Quivy, M. Harmelin, and A. M. Flank, J. Non-Cryst. Solids **65**, 109 (1984).

[61] M. H. Cohen and G. S. Grest, Phys. Rev. B **20**, 1077 (1979).

[62] J. D. Honeycutt and H. C. Andersen, J. Phys. Chem. **91**, 4950 (1987).

[63] H. Jonsson and H. C. Andersen, Phys. Rev. Lett. **60**, 2295 (1988).

[64] D. W. Qi and S. Wang, Phys. Rev. B **44**, R884 (1991).

[65] K. Chen, H. Liu, and Z. Hu, J. Phys.: Condens. Matter **7**, 517 (1995).

[66] H. Li, G. Wang, X. Bian and F. Ding, Phys. Rev. B **65**, 035411 (2001).

[67] H. Li, G. Wang, J. Zhao, X. Bian, J. Chem. Phys. **116**, 10809 (2002).

[68] J. H. He and E. Ma, Phys. Rev. B **64**, 144206 (2001).

[69] H. W. Sheng, J. H. He, and E. Ma, Phys. Rev. B **65**, 184203 (2002).

[70] T. C. Hufnagel and S. Brennan, Phys. Rev. B **67**, 014203 (2003).

[71] K. Saksl, H. Franz, P. Jovari, K. Klementiev, E. Welter, A. Ehnes, J. Saida, A. Inoue, and J. Z. Jiang, Appl. Phys. Lett. **83**, 3924 (2003).

[72] A. Di Cicco, A. Trapananti, S. Faggioni, and A. Filipponi, Phys. Rev. Lett. **91**, 135505 (2003).

[73] W. K. Luo, H. W. Sheng, F. M. Alamgir, J. M. Bai, J. H. He, and E. Ma, Phys. Rev. Lett. **92**, 145502 (2004).

[74] K. Ahn, D. Louca, S. J. Poon, and G. J. Shiflet, Phys. Rev. B **70**, 224103 (2004).